

Assessment of satellite aerosol optical depth over Greater Bangkok during 2003–2018

Nitchanan Nantawong^{1,2}, Nishit Aman^{1,2}, Kasemsan Manomaiphiboon^{1,2*},
Peerapol Chankasem^{1,2}, Vanisa Surapipith³ and Awassada Phongphiphat^{1,2}

¹The Joint Graduate School of Energy and Environment, King Mongkut's University of Technology Thonburi, Thailand

²Center of Excellence on Energy Technology and Environment, Ministry of Higher Education, Science, Research, and Innovation, Thailand

³Atmospheric Research Unit, National Astronomical Research Institute of Thailand

*Corresponding author: kasemsan.jgsee@gmail.com, Tel.: +66 2 470-7331

Abstract: This study characterizes aerosol optical depth (AOD) over Greater Bangkok (GBK) and nearby regions in Central Thailand (CT) using MODIS–Aqua AOD data for a period of 16 years (2003–2018). AOD and PM_{2.5} show a linear relationship but its strength is small to fair, suggesting the contrast between the column-integrated and surface-level quantities. On a monthly scale, both GBK and CT show similar patterns for AOD variation (for both average and extreme). AOD in GBK is higher than that in CT due possibly to larger anthropogenic emissions. AOD is relatively low in the wet season due to the stronger wind and scavenging effect of rain. AOD peaks in March and October. The former peak is attributed to biomass burning for land clearing before wet-season cropping and more secondary aerosols induced by warm and humid conditions. The latter peak is due possibly to increased biomass burning in the late wet season for land clearing to support dry-season cropping since large irrigated areas are well present within CT. Dry-season AOD tends to intensify most and spread over large areas in February–April. Based on spatial correlation analysis, haze management for GBK in December and January needs to consider areas outside GBK. During February–April over the recent years, increased AOD in GBK, despite decreased biomass burning, is observed and likely to be induced by urbanization and economic growth but increased AOD in CT is thought or speculated to be more linked with unfavorable meteorological conditions. The developed multiple linear regression model to relate AOD in GBK and meteorology explains 43% of total variability in dry-season AOD. The important input meteorological variables remaining in the final regression include persistence, cloud cover, relative humidity, wind speed, and westerly wind. Persistence shows positive association with AOD, suggesting haze problems to be multi-day events.

Keywords: Air quality, urbanization, seasonality, spatial coherency, fires.

1. Introduction

Atmospheric aerosols are solid and liquid particles suspended in the air. They are released either by natural processes (e.g., volcanic eruption, dust storm, and sea spray) or by anthropogenic activities (e.g., fuel combustion, biomass burning, agricultural activities, transportation, and industrial processes) [1]. Effects of atmospheric aerosols on human health have been well reported [2-4]. Aerosols can affect surface energy balance in multiple ways. For direct effects, they scatter and absorb sunlight, resulting in reduced solar radiation reaching the surface. Through indirect effects, being more complex than the direct effects, aerosols can act as cloud condensation nuclei (CCN) and alter cloud optical properties, cloud droplet size, and population, in turn affecting precipitation and water cycles [1]. How aerosols affect weather and climate, as well as its uncertainty, has been commonly known as an important scientific subject. Aerosol optical depth (AOD) is a physical property of aerosols, which is defined as the total light extinction in the vertical column due to the scattering and absorption of light over the unit cross-sectional area and can thus be related to particulate matter as an essential air pollutant. It is measured using a ground-based sun-photometer (either fixed or portable) or derived from satellite data [5-7]. During a recent couple of decades, satellite AOD has been monitored and intensively used for studying aerosols at various spatiotemporal scales and long-term trends [8-12], and understanding aerosol types in a region [13-14]. Satellite AOD can also be used to estimate

surface particulate matter, especially particles smaller than or equal to 2.5 μm and 10 μm in size (shortly, PM_{2.5} and PM₁₀, respectively), but their relationship may not be straightforward and can be complicated by many factors [15-16]. Surface PM_{2.5} estimation using satellite AOD has been widely studied by means of statistical models with meteorology, land cover, and socio-economic factors as input [17-20].

Bangkok, the capital of Thailand, and its five neighboring provinces (Nakhon Pathom, Nonthaburi, Pathumthani, Samut Prakan, and Samut Sakhon), collectively known as Greater Bangkok (GBK) (Figure 1), represent the largest urban agglomeration in Thailand and also one of the largest in Southeast Asia. Its continuous growth and urbanization have negatively affected environmental conditions, including air quality [21]. The degradation of air quality was typical of concern in the dry season when weather conditions tend to be favorable to air pollutants to elevate. For PM_{2.5}, its levels have exceeded the daily (i.e., 24-h average) national ambient air quality standard (NAAQS) of 50 $\mu\text{g m}^{-3}$ multiple times annually [21].

A limited number of AOD studies have still been conducted in Thailand as compared to PM and ozone pollution studies. For example, Janjai et al. (2009) [5] and Janjai et al. (2012) [6] reported higher AOD during summer (March–April) based on their investigation of daily and seasonal AOD variations at multiple sites. Bridhikitti (2013) [22] examined atmospheric aerosol layers over Greater Bangkok using satellite AOD and attributed elevated dry-season haze to long-range transport of air pollutants. Kanabkaew

et al. (2013) [23] used MODIS (Moderate Resolution Imaging Spectroradiometer) AOD data and surface meteorological data to predict hourly $PM_{2.5}$ in Chiang Mai, the largest city (in terms of population and economy) in the northern region. Zeeshan and Kim Oanh (2014) [24] suggested the dependence of PM_{10} and AOD correlation on synoptic patterns and mixing height. Sukitpaneevit and Kim Oanh (2014) [25] reported a moderate-to-good correlation between satellite AOD and CO with surface PM_{10} and CO, respectively, in the dry season for Chiang Mai.

Here, the latest MODIS Collection 6.1 (C6.1) aerosol product from the Aqua satellite of the NASA (National Aeronautics and Space Administration) was used to investigate AOD characteristics for GBK and also the central region or Central Thailand (CT), including spatiotemporal variation, spatial coherency, epochal AOD comparison, and statistical relationship with meteorological variables. To our knowledge, this long-term assessment of satellite AOD will complement the existing knowledge and understanding of atmospheric aerosols for GBK.

2. Study Area

As mentioned previously, GBK is the focused area for the

current assessment. Its gross provincial product (GPP) (defined as the national gross domestic product or GDP but scaled to a provincial level) [26], energy consumption [27], and population [28] apparently show growth over the last two decades (Figures 2a–c). Urbanization has continuously increased, with a faster rate seen in GBK than in Bangkok (Figure 2d). To facilitate the assessment, three grids were defined, namely CT, GBK, and urban core (UC) grid (based on the spatial resolution of the MODIS–Aqua AOD data, see below) (Figures 3a 3b).

The general climate in GBK or CT follows that of the upper part of Thailand, which is tropical and humid. It is mainly regulated by the two prevailing monsoons: northeast (November–February) and southwest (May–October) [29]. The former monsoon brings cool dry air (i.e., the winter). The latter monsoon brings moist air from the Indian Ocean and the Gulf of Thailand, causing abundant rain (i.e., the wet or rainy season). The transitional period of March–April has the warmest condition (i.e., the summer). The dry season, referred herein, constitutes the winter and summer seasons. It is noted that the dry season has an important synoptic feature called cold surge, which is characterized by abrupt moderate-to-strong winds with cool dry air from the mid-latitudes southward or southwestward to the Indochina Peninsula [30].

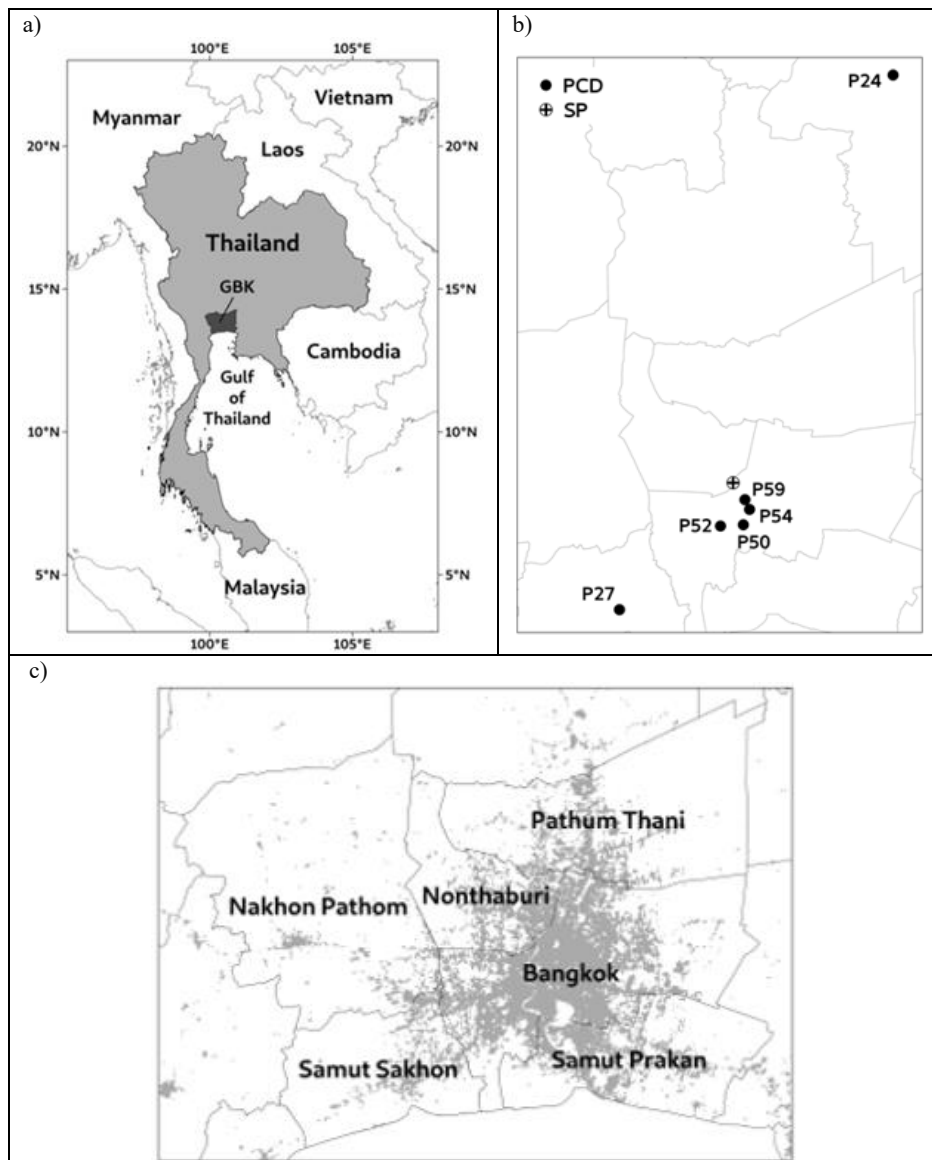


Figure 1. a) Thailand, b) PCD stations and sun-photometer site, c) Greater Bangkok and its provinces. The grey shading indicates built-up areas.

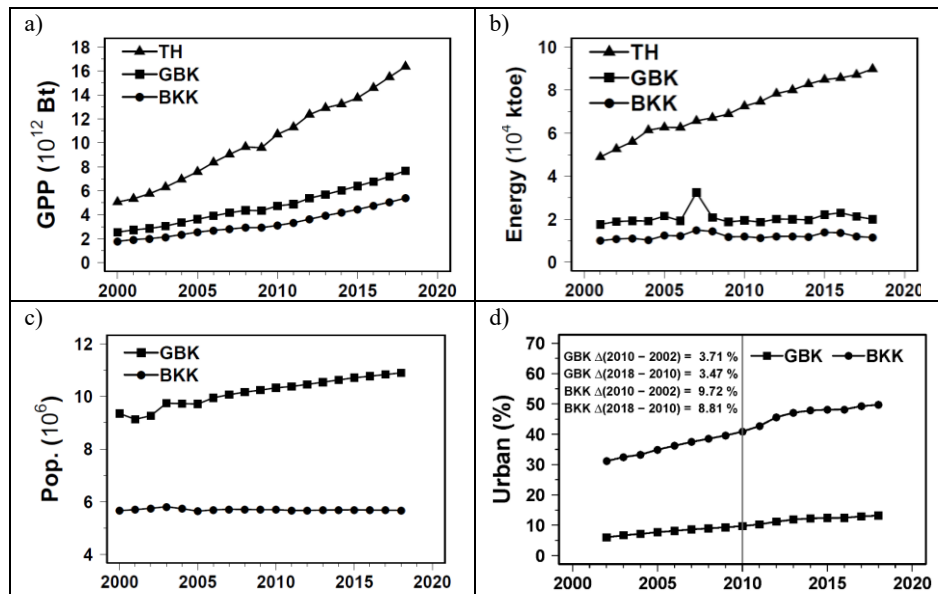


Figure 2. a) Gross Provincial Product (GPP) (at current market price) b) energy consumption (in units of 10^4 ktoe and 1ktoe = $41,868 \times 10^9$ J), c) registered population, and d) total urban area (%). The acronyms TH, GBK, and BKK stand for Thailand, Greater Bangkok, and Bangkok, respectively.

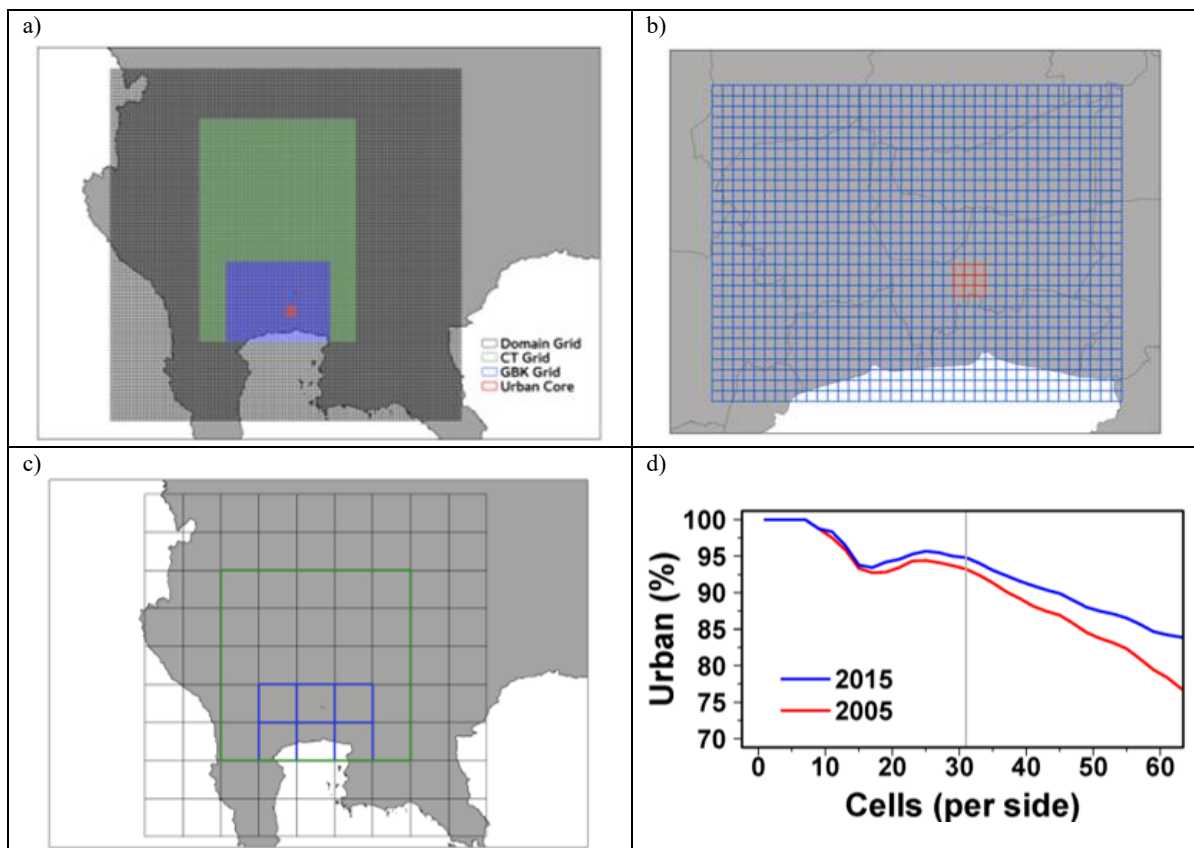


Figure 3. a) Grids considered in this study (black: full domain, green: CT, blue: GBK, and red: UC), b) GBK grid with the red grid cells (shortly, pixels) corresponding to UC, c) CFS grid with the blue pixels corresponding to GBK, and d) total urban area (%) versus the size of a UC-centered box in units of land-cover (ESA CCI) pixels. Here, a box of 31×31 pixels is shown to properly represent UC.

3. Data

The MODIS sensors on board of the Terra and Aqua satellites, both combined, pass and cover the entire Earth every 1 to 2 days, and they acquire data in 36 spectral channels at multiple spatial resolutions (250 m, 500 m, and 1000 m) [7]. Two global AOD products at 3-km and 10-km resolutions are produced by

the MODIS Adaptive Processing (MODAPS) with Dark Target (DT) algorithm to estimate AOD at the 3-km resolution and with both Dark Target (DT) and Deep Blue (DB) algorithms for the 10-km resolution [7]. The latest MODIS-Aqua Collection 6.1 (C6.1) Level-2 AOD 3-km product (MYD04_3K) from the DT algorithm (available at <https://ladsweb.nascom.nasa.gov/>) was adopted for use here but only for daytime overpasses. A total of

16 seasonal years (2003–2018) were considered. For example, the seasonal year 2003 is defined as starting in November 2002 and ending in October 2003, with the dry season covering November 2002 to April 2003 and the wet season covering the remaining months. Moreover, two epochs were defined and used for comparison between the past and recent periods, which are EP1 (2003–2010) and EP2 (2011–2018). The most interested variable extracted is “Optical Depth Land and Ocean” (at 0.55 μm), already filtered for quality assurance and ready for use [7]. The Level-2 MODIS data are swath-based. Thus, they were re-gridded using HDFLOOK software (available at <http://loawwww.univ-lille1.fr/SOFTWARE/Hdflook>) to a regular latitude–longitude grid. In our data processing, if any pixel reports valid values from different swath files on the same day along the same daytime overpass, averaging is applied. Because the downloaded data have been quality-filtered (including cloud contamination), large percentages of missing data were found (more in the wet season). For statistical calculation in this study, monthly AOD at a particular pixel was computed (e.g., pixel-wise average and 95th percentile) using valid daily AOD values (at least 5% required) at the pixel in a particular month. Average AOD over an area was computed using valid values found from all pixels in the area (at least 50% required).

A set of ground-based AOD set, measured by a portable sun-photometer (SP), was obtained from Aman (2019) [31] in order to compare with the MODIS AOD data. The measurement site is at the rooftop (44 m agl) of a building at the King Mongkut of Technology North Bangkok (KMUTBN) (Figure 1b and Table 1). The dataset covers hourly daytime AOD values during January–March of 2014 and 2015. The portable SP has five spectral channels (440 nm, 500 nm, 675 nm, 870 nm, and 936 nm). The instrument was placed onto a tripod for handling security. Since clouds directly affect AOD observation, any cloudy days were removed. The technical details of the AOD measurement are referred to Aman (2019) [31]. Since the wavelength pertaining to MODIS AOD reported is 550 nm, the following equation was employed to adjust SP AOD at 500 nm to 550 nm:

$$\tau_{550} = \tau_{500} \times \left(\frac{0.55}{0.5}\right)^{-\alpha}, \quad (1)$$

In equation 1, τ_{500} and τ_{550} are the AOD values at 500 nm and 550 nm, respectively, α is the Angstrom exponent calculated using a linear fit to the logarithmic form of the following Angstrom formula:

$$\tau_{\lambda} = \beta \lambda^{-\alpha}, \quad (2)$$

In equation 2, τ_{λ} is the AOD value at wavelength λ , α is the Angstrom exponent, and β is the turbidity coefficient.

Hourly surface PM_{2.5} data were requested and obtained from the Pollution Control Department (PCD) for six air quality

monitoring stations located in the study area (Figure 1b and Table 1) for comparison with the AOD data. These stations have good adequacy of reported data. It is noted that air-quality data collected at stations are internally quality-inspected by the PCD before public release. Typically, at a PCD station, an air sampler is placed at an approximate height of 3 m agl and PM_{2.5} is continuously detected using beta gauge attenuation (Figure S1 in Supplementary Materials). It is noted that, after the temporal and spatial collocation of the PM_{2.5} data with the satellite AOD data, only three stations were chosen for use (P24, P52, and P54) because the other stations gave relatively low pairings.

Meteorological data used were extracted from 0.5°-resolution hourly Climate Forecast System (CFS) reanalysis data [33, 34], which include air temperature (T), precipitation (PP), planetary boundary layer height (PBLH), cloud cover (CC), relative humidity (RH), and wind (at 10 m agl and 925 mb). Only the data from 13 LT and 15 LT were used, corresponding to the overpass times of the Aqua satellite during the daytime above CT (12.67–14.67 LT with a mean of 13.63 LT) (Figure S2 in Supplementary Materials). The pressure level of 925 mb is equivalent to about 760 m msl, approximately the middle of the PBL in the tropics. It is noted that 925-mb wind was mainly used because it represents wind for the bulk PBL than 10-m wind, which is suitable for column-integrated AOD. To examine how biomass burning (forest and agricultural fires affect AOD, daily 1-km active fires detected by MODIS [35] were used, here MCD14ML Collection 6 that combines fires detected by MODIS on the Terra and Aqua satellites, (available at <https://firms.modaps.eosdis.nasa.gov/download/>). For the land cover, satellite-derived yearly land cover data from the European Space Agency Climate Change Initiative (ESA CCI) were used (available at <http://www.esa-landcover-cci.org/>). The dataset has a 300-m resolution and 22 land cover classes, based on the classification of the Food and Agriculture Organization (FAO).

A number of grids (full domain, CT, GBK, and UC) were specified in support of the assessment. Their grid resolutions (i.e., pixel sizes) correspond to those of data (here, MODIS AOD and CFS) overlaid upon. The UC grid represents the urban core of GBK, for which urbanized (i.e., built-up) areas are dominant. It was defined as follows: A location (13.75° Lat. and 100.56° Lon.) is marked as the city center. Next, the percentage of total urbanized areas found in the land-cover (ESA CCI) data is computed within a box with varying size (number of 300-m pixels per size = 1, 3, 5, 7, 9, ..., and so on sequentially) and plotted (Figure 3d). As seen, a sharp decrease in total urbanized areas is first encountered at the box size of 31×31 pixels, which is sufficient to designate it as UC. The box size is approximately equivalent to 9×9 km² and 3×3 MODIS AOD pixels. From the plot, the UC grid does not change with the year (e.g., 2005 and 2015) and is reasonably valid for use over the full period considered.

Table 1. Surface PM_{2.5} and sun-photometer stations.

Station	Source	Name (Province)	Lat. (deg.)	Lon. (deg.)	Period	Background
24 (used)	PCD	Na Phra Lan (Saraburi)	14.68634	100.87172	2013–2018	General
27	PCD	Samut Sakhon Wittayalai school (Samut Sakhon)	13.55035	100.26473	2013–2018	General
50	PCD	Chulalongkorn Hospital (Bangkok)	13.72983	100.53649	2017–2018	Roadside
52 (used)	PCD	Electricity Sub-Station Thonburi (Bangkok)	13.72747	100.53649	2016–2018	Roadside
54 (used)	PCD	Community Housing Authority Din Daeng (Bangkok)	13.7625	100.53649	2011–2018	Roadside
59	PCD	Public Relations Department (Bangkok)	13.7833	100.54041	2015–2018	General
SP	Aman (2019)	KMUTNB (Bangkok)	13.8194	100.5147	2014–2015	Rooftop (44 m agl)

Remark:

PCD: Pollution Control Department

SP: Portable sun-photometer

Table 2. List of the data used in the study.

Variables	Sources/ Developers	Resolution	Frequency	Period
MODIS AOD	LAADS (NASA)	0.027° (~3 km)	Daily (afternoon)	2002–2018
Land cover (22 classes)	ESA CCI	0.00277° (~0.3 km)	Yearly	2002–2018
Air temperature (K)	CFS, NCEP/NOAA	0.5°	Hourly	2002–2018
Cloud cover (%)				
Planetary Boundary Layer Height (m)				
Precipitation (mm s ⁻¹)				
Relative Humidity (%)				
10–m wind (m s ⁻¹) 925–mb wind (m s ⁻¹)				
Remark:				
LAADS: Level-1 and Atmosphere Archive and Distribution System				
NASA: National Aeronautics and Space Administration				
ESA CCI: European Space Agency Climate Change Initiative				
CFS: Climate Forecast System Reanalysis (CSFR till Mar. 2011, and CFSv2 since Apr. 2011)				
NCEP/NOAA: National Centers for Environmental Prediction/National Oceanic and Atmospheric Administration, US				

4. Results and Discussions

4.1 AOD and PM_{2.5} Comparison

In comparison between MODIS AOD and SP AOD, pixel–point collocation is necessary. To sustain the number of samples, temporal and spatial collocation has been done differently in previous studies. Nichol and Bilal (2016) [36] used an average AOD between 12 LT and 14 LT for 3×3 pixels centered over a ground–based site. Likewise, Bilal et al. (2019) [37] used the same spatial collocation but only times within one hour of the satellite overpass. Gupta et al. (2018) [38] used average AOD over 0.15°×0.15° within half an hour of the satellite overpass. Since the mean of Aqua satellite overpass during the daytime over CT is 13.63 LT. Thus, SPAOD observed at 14 LT was used.

For the spatial collocation, like Gupta et al. (2018) [38], average AOD within 0.15°×0.15° centered at the measurement site was used, and a total 46 days were available for comparison (Figure 4a). The correlation between MODIS AOD and SP AOD is shown to be reasonably high (0.84) with the majority of their data pairs falling within the factor–of–two envelope, suggesting the applicability of MODIS AOD. Comparing between MODIS AOD and PM_{2.5} at the chosen three stations, a positive correlation is small to fair (0.25–0.33) (Figures 4b–d). Since PM_{2.5} is measured near the surface while AOD is a column–integrated quantity, their relationship is not necessarily linear and is influenced by many factors [15–16]. Aman (2019) [31] also reported the influence of relative humidity and wind on the relationship of PM₁₀ and AOD for Bangkok.

4.2 Temporal and spatial variation

The monthly variation of average AOD appears to be similar for both GBK and CT and also in both epochs (EP1 and EP2) (Figure 5), with higher values found in GBK. AOD is generally relatively high in the dry season, compared to the wet season, with two peaks (the higher one in March and the lower one in October). Extreme (here, 95th percentile) AOD also displays a similar pattern to average AOD, i.e., higher values seen in GBK. These suggest intense human activities in GBK that lead to strong anthropogenic emissions. The March peak is attributed to biomass burning being the most intensified in March, corresponding to the typical time of land preparation for the next cycle of cropping or to start in the beginning of the wet season (see Figure S3 in Supplementary Materials) [39]. Another possible factor is the increased secondary aerosols due to warmer and also more humid conditions during the summer (Figure S4a in Supplementary Materials). Relatively low AOD in the wet season is generally caused by stronger wind (i.e., better atmospheric ventilation) and scavenging rain (Figure S4 in Supplementary Materials). A similar monthly variation of AOD in GBK has been reported by previous studies [5–6]. The October peak of AOD is quite interesting despite well–present rain and somewhat limited fire hotspots observed (Figures S3 and S4 in Supplementary Materials). Although no clear explanation is given here, its possible reasons include increased agricultural burning to get rid of crop residues for off–season cropping starting in the early dry season [40]. This practice is relevant to irrigated land which is abundantly present in CT.

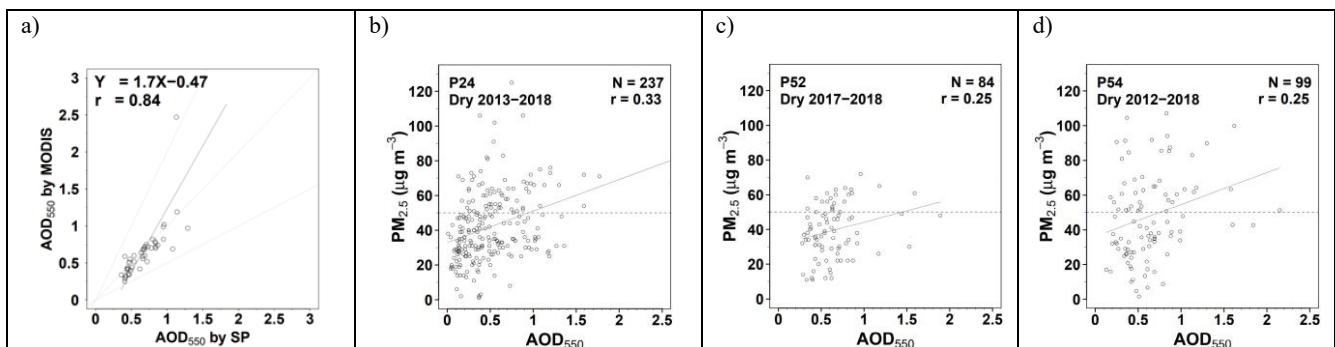


Figure 4. a) Comparison of SP AOD and MODIS AOD at 550 nm, and b–d) comparison between MODIS AOD and PM_{2.5} in the dry season at the chosen three PCD stations. In each plot, the solid line is the linear fit. The middle dashed line is of the 1:1 slope. In a), the top and bottom dashed lines are the factor–of–two lines.

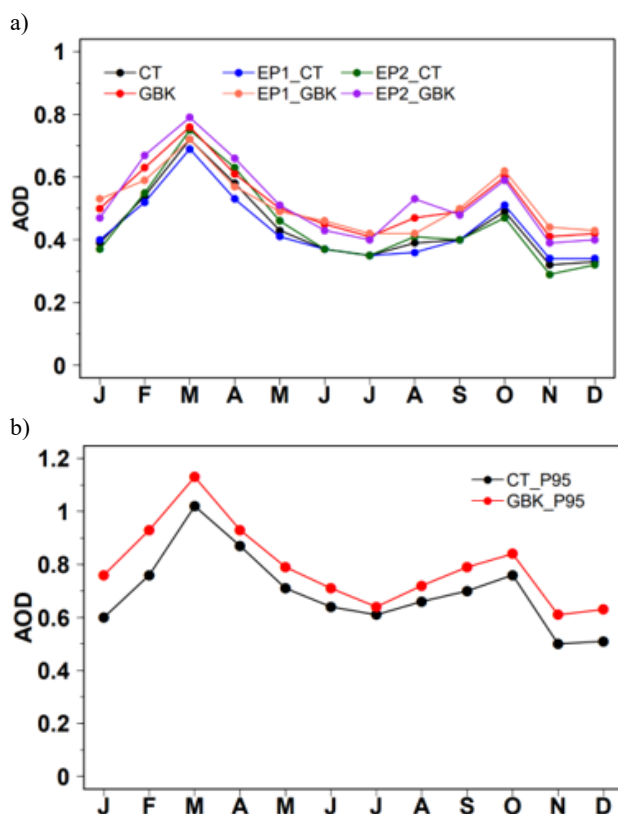


Figure 5. a) Monthly mean land AOD and b) monthly high-end (95th percentile) AOD over CT and GBK. EP1 and EP2 are the first and second half-periods of 2003–2018.

Monthly AOD over the full domain was also mapped (Figure 6). A contrast in intensity and distribution between the first half of the dry season (November to January) and the second half (February to April) is apparent. That is, the first half has a lesser degree but AOD becomes considerably intensified in the second half, as in the above-discussed results in Figure 5. The two peaks are also exhibited in the March and October maps. It is noted that the maps in the wet-season months have more missing pixels shown since valid data are less available in the data product because of cloud screening. But such burning is not readily detected by optical satellite sensors due to cloud obstruction, which is likely our current case of MODIS fire hotspots in October. Nevertheless, Junpen et al. [40] alternatively used a MODIS burnt-area product and also found substantial burning in this month.

4.3 Spatial coherency

To determine how dry-season AOD in the city center (i.e., UC) is spatially coupled with that in its vicinity, a correlation between their daily AOD was computed (Figure 7). This information is useful in that it helps suggest whether haze management should be limited to just the GBK, given that the AOD condition is not static but changes with month. It is seen from the figure that correlation decreases with distance from UC. However, when examining closely to areas with significantly high correlation (>0.75), we found that such areas is mostly constrained within GBK in every month, except December and January when the high correlation is seen outside GBK to the north and to the southeast. These results indicate haze in GBK in these two months may not be possible to manage within GBK but needs to extend to its surroundings as one larger coherent domain. Northeasterly 925-mb wind observed during these two months could effectively transport aerosols from biomass burning outside GBK to the north (Figures 7 and Figure S5 in Supplementary Materials). Although wind direction in January does not show a direct link AOD between GBK and Eastern Thailand, other factors may influence their linkage or association, e.g., horizontal turbulent dispersion and secondary aerosol formation. In the other dry-season months, haze tends to be GBK-constrained, and its mitigation may emphasize emissions within GBK. A similar study by Kumar et al. (2013) [9] identified a homogeneous region of aerosols within a certain radial distance using spatial correlation and found such a region to be asymmetrical and skewed toward coastal areas.

4.4 Epochal comparison

Monthly AOD and its differences between EP1 and EP2 were quantified for GBK (Figure 8). Although AOD varies with year and month, it tends to be relatively high in the second half of the dry season (February–April). The years 2011 and 2016 have the most intensified levels.

Comparing the two epochs, it is evident that AOD worsens over the recent years (i.e., EP2). CT does not have substantial increases in biomass burning (in terms of fire hotspots) in the dry season between the two epochs (Figure S3 in Supplemental Materials). Specifically, biomass burning decreases in almost all of the dry-season months (5 out of 6), with only April having an increase by 27%. The AOD increase found in GBK is thus attributed mainly to its urbanization and economic growth, consistent with the data in Figure 2. Nevertheless, the spatial examination of AOD over the CT reveals that AOD turns out to aggravate in February–April over most parts of CT (i.e., not limited to just GBK) (Figure 9). Since most of CT is vegetative (e.g., agricultural and forest) and not urbanized but still has the AOD increase, it is argued or speculated that meteorology could play an important role. However, this argument is based on our general point of view, comprehensive investigation with year-to-year meteorological variation is required to address the issue adequately.

Table 3. Regression results of dry-season AOD in GBK.

$AOD_{dry} = 0.477 + \mathbf{0.465 PER} + 5.62 \times 10^{-4} CC - 4 \times 10^{-3} RH - 4 \times 10^{-3} WS - \mathbf{0.207 WD(W)}$	$R^2 = 0.428$
Coefficients (corresponding p -values):	($N = 330$)
Intercept (< 0.001), PER (< 0.001), CC (< 0.1), RH (< 0.01), WS (< 0.01), and WD (W) (< 0.05)	

Remark:

- The final variables in the regression are shown above. The non-bold and bold letters mark statistical significance at 0.1 and 0.05 levels, respectively.
- N is the number of days used in the regression.
- PER is the persistence (here, previous-day AOD).
- WS and WD are of the vector-average (over 13–15 LT) 925-mb wind speed and direction, respectively.
- All variables are numeric and continuous, except for WD treated as categorical (N, NE, E, SE, S, SW, W, and NW). Among all these directions, only WD(W) is the wind direction found to be statistically significant, and its total effect on AOD simply equals its coefficient whenever wind is westerly (blowing from the west) (otherwise, zero). Given the negative coefficient, the westerly wind tends to reduce AOD.

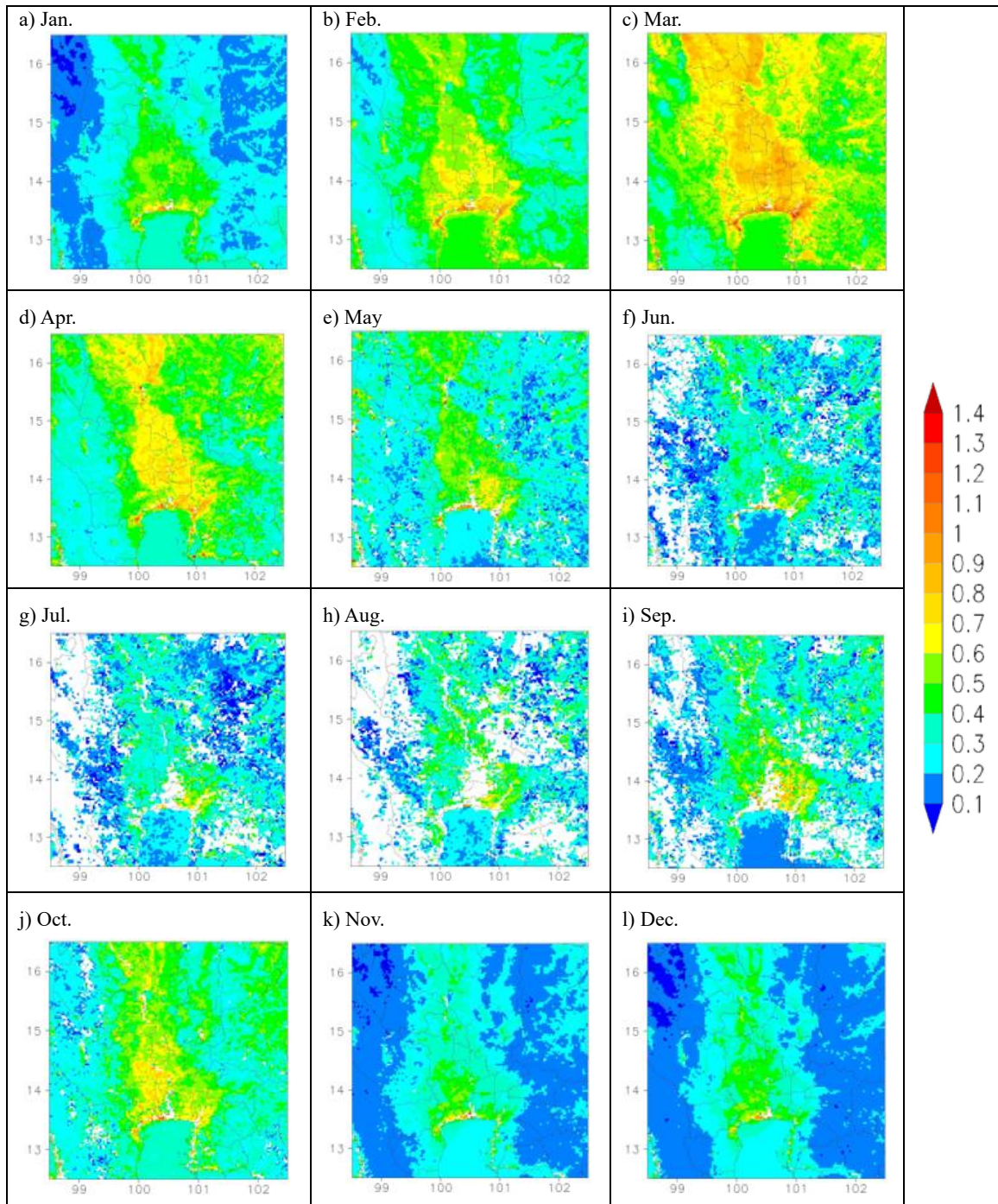


Figure 6. Monthly mean AOD over 2003–2018 (as seasonal years). Missing pixels are marked by white pixels.

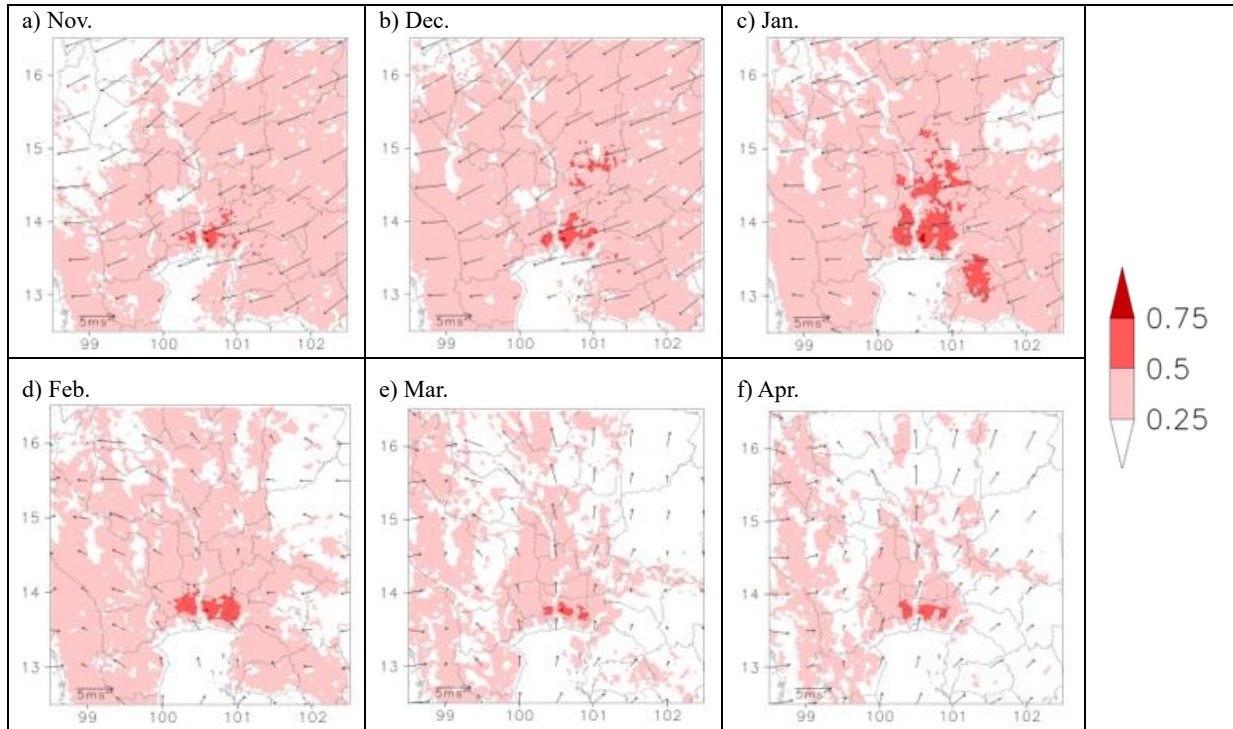


Figure 7. Monthly dry-season correlation between AOD at each individual pixel and that at UC. The wind vectors are at 925 mb.

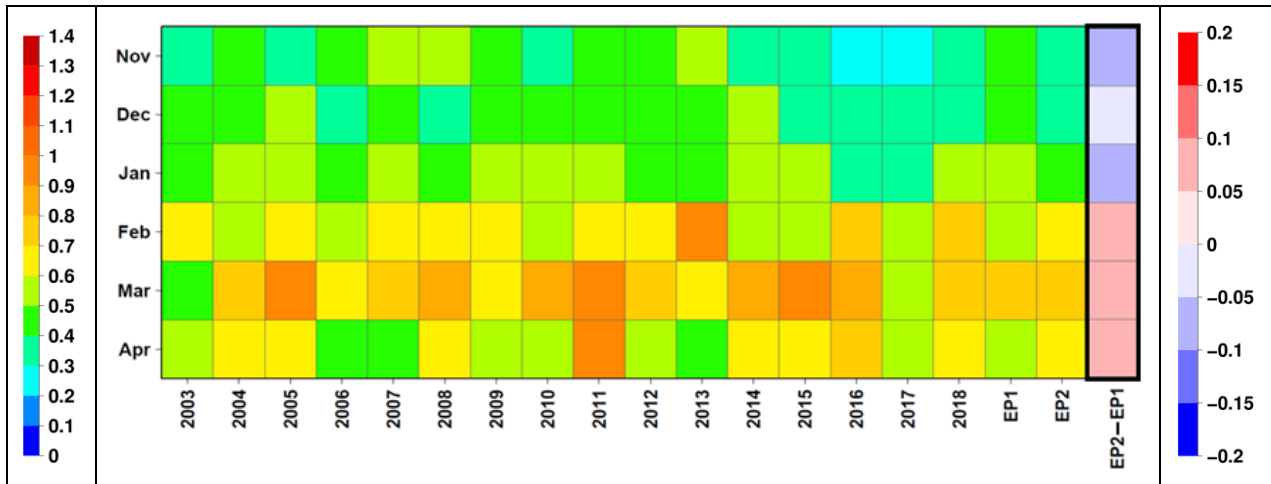


Figure 8. AOD over GBK by seasonal year and month.

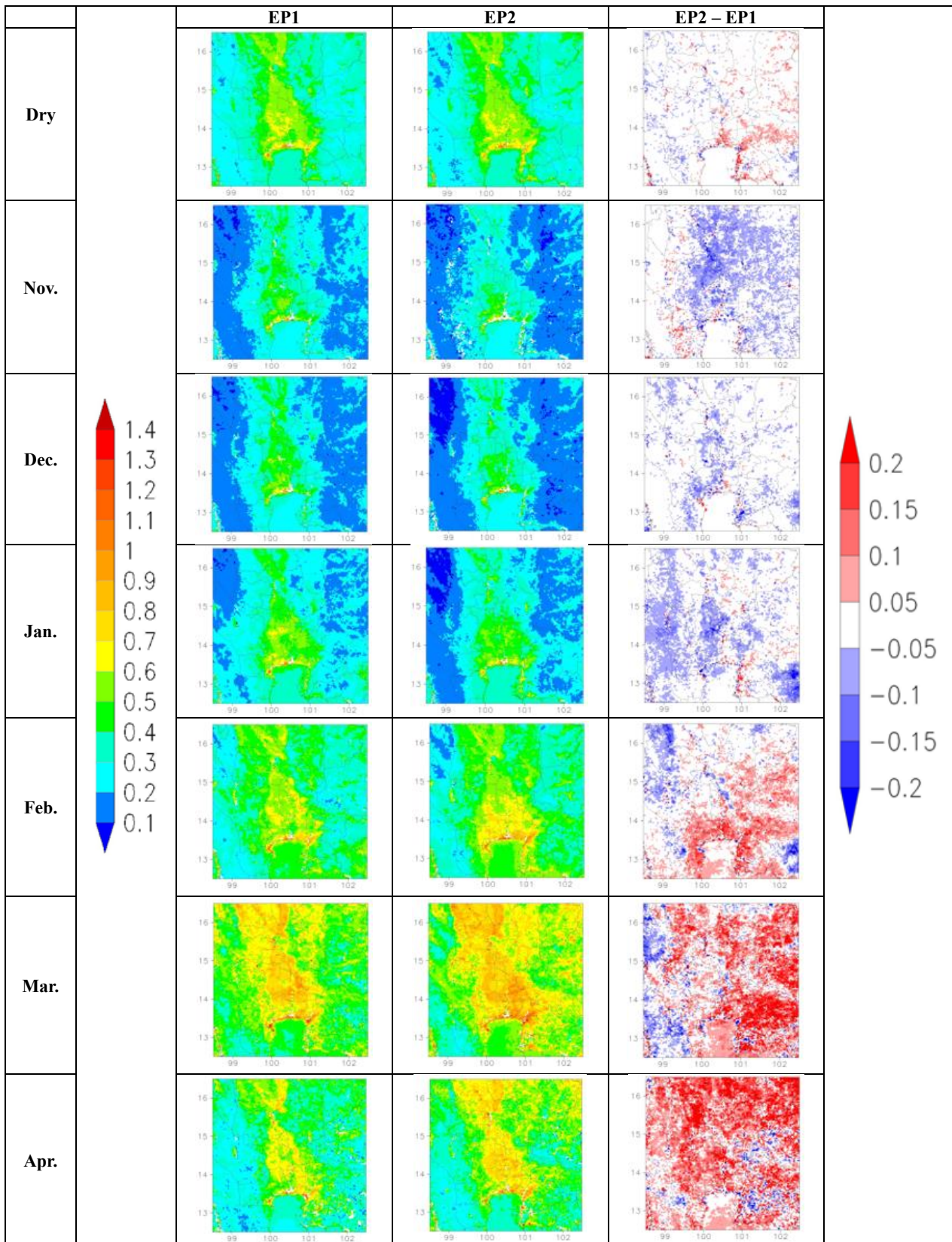


Figure 9. Dry-season AOD in EP1 and EP2 and difference (EP2 – EP1).

4.5 Meteorological effects

To understand the effects of meteorology on dry-season AOD in GBK on a daily basis, the statistical relationship of AOD with a set of selected meteorological variables using multiple linear regression (MLR) was formulated. The MLR is a widely

used simple method in both doing so and air pollution forecasting [41-44]. For example, Tan et al. (2016) [43] used the technique to predict AOD for Penang Island Malaysia. Jiang et al. (2018) [44] identified factors affecting AOD in Jiangsu China, some of which include socio-economic indicators. The method involves

a linear relationship between response (predicted) and explanatory (or predictor) variables. Here, a set of eight daily predictors was initially selected, including cloud cover (CC), planetary boundary layer height (PBLH), relative humidity (RH), temperature (TEMP), wind speed (WS), wind direction (WD), fire hotspot count, and persistence (PER). WD is categorical as eight sectors as follows: northerly (N), northeasterly (NE), easterly (E), southeasterly (SE), southerly (S), southwesterly (SW), westerly (W), and northwesterly (NW). PER was incorporated to reflect the effect of the previous (i.e., background) condition, here previous-day. Stepwise backward elimination, as in Aman et al. (2019) [45], was employed to obtain the final (as parsimonious and optimal) MLR model (Table 3), whose residual diagnostics (here, independent error, normality of error, homoscedasticity of error, and outlier leverage) were found to be fairly acceptable. The MLR was implemented using the built-in “lm” function of the R software [46].

The final model captures 42.8 % of the total variability in the original AOD data using the following five variables (PER, CC, RH, WS, and WD(W)). The presence of PER in the final model with a positive association with AOD highlights that haze pollution in GBK tends to be multiple-day episodic, as opposed to single-day events. CC has a positive association while RH and WS have a negative association. More clouds indicate more chance of rain but the dry season has limited rain anyway. Thus, more clouds may as well lead to reduced global radiation, more near-surface atmospheric stability, less mixing or dilution of airborne constituents, and then more accumulate of aerosols. Moreover, as a positive feedback, aerosols can act as cloud condensation nuclei (CNN), and more aerosols yield more clouds if humidity is present enough. Humidity in GBK is typically associated with rain and moisture-laden wind from the Gulf of Thailand, helping scavenging aerosols. However, humidity is well known to enhance or promote the secondary aerosol formation, which is not possible to explicitly account for by the current MLR model. It is straightforward that stronger wind ventilates the atmosphere more efficiently, as opposed to stagnant conditions. For wind direction, only westerly wind is maintained with a negative association.

It is noted that the developed statistical model explains about 43% of AOD variance and the remaining variance is still not captured. Further model improvement possibly requires additional input variables that potentially influence AOD. For example, meteorological variables are upper-air wind, mixing height, synoptic pattern, local recirculation, and air-mass pathway. Certain socio-economic variables may also be considered, e.g., population, energy usage, and land cover.

5. Conclusions

In this study, aerosol characterization over Greater Bangkok (GBK) and nearby regions in Central Thailand (CT) was carried out using the latest MODIS Aqua Collection 6.1 (C6.1) Level-2 AOD (aerosol optical depth) data for the years 2003–2018. Although AOD and PM_{2.5} show a linear relationship, its strength is small to fair, suggesting intrinsic limitation or contrast between the column-integrated and surface-level quantities. On a monthly scale, both GBK and CT show similar patterns for AOD variation (for both average and extreme). AOD in GBK is higher than that in CT due generally to larger anthropogenic emissions. AOD becomes relatively low in the wet season due to the stronger wind and scavenging effect of rain. The double peaks in AOD in March and October are observed. The former peak is attributed to biomass burning for land clearing before wet-season cropping and more secondary aerosols induced by warm and humid conditions. The latter peak due possibly to increases biomass burning in the late wet-season to prepare land for dry-season cropping since large irrigated areas are well present within

CT. In the dry season, AOD tends to intensify most and spread over large areas in February–April. The spatial correlation analysis indicates that haze management for GBK in December and January needs to consider areas outside GBK. During February–April over the recent years, increased AOD in GBK, despite decreased biomass burning for most of the months, is observed and likely to be induced by urbanization and economic growth but increased AOD in CT is speculated or thought to be more linked with unfavorable meteorological conditions (subject to further investigation). The developed multiple linear regression model explains 43% of total variability in dry-season AOD in GBK with five meteorological variables, including persistence, cloud cover, relative humidity, wind speed, and westerly wind. Persistence shows positive association with AOD, suggesting haze problems to be multi-day events. Cloud cover reduces global radiation to the surface, increases low-level atmospheric stability, and in turn promote the accumulation of pollutants. Relative humidity is more likely to link to rain and its scavenging effect. Stronger winds offer better atmospheric ventilations. Among all wind directions, only the westerly winds are significantly shown to alleviate the pollution in the study area.

The present study acknowledges a number of technical limitations. Although satellite AOD is useful, it suffers from a relatively high amount of missing data. AOD is a column-integrated quantity and then does not represent surface particulate pollution directly, which is more relevant in the context of air pollution and its impact on public health. The source of regional meteorological data considered is reanalysis data whose relatively coarse resolution may not suit urban-scale studies such as this study. Future work can extend to resolve the mentioned limitations and also the following aspects: use of different satellite AOD products for uncertainty analysis or data merging, consideration of satellite-based aerosol types, a sophisticated statistical relationship of satellite AOD relationship with PM_{2.5} together with additional input variables, back-trajectory analysis of potential long-range transport [47], and numerical urban-scale modeling [48].

Acknowledgements

The authors sincerely thank the Pollution Control Department (PCD) for providing the surface PM_{2.5} data and Assoc. Prof. Wongpun Limpaseni for his useful perspectives given to the study. This study was supported by the Joint Graduate School of Energy and Environment (JGSEE), the Postgraduate Education and Research Development Organization (PERDO), the National Research Council of Thailand (NRCT), the Hydro-Informatics Institute (HII), and the Energy Conservation and Promotion Fund (ENCONFUND) of the Ministry of Energy. We also extend our thanks to an anonymous reviewer for the useful comments.

Conflicts of Interest

The authors declare no conflict of interest.

Supplementary Materials

The supplement information of this article is available at <http://www.jseejournal.com>.

References

- [1] Seinfeld, J.H. and Pandis, S.N. 2006. *Atmospheric Chemistry and Physics: From Air Pollution to Climate Change*, Wiley.
- [2] Kampa, M. and Castanas, E. 2008. Human health effects of air pollution, *Environmental Pollution*, 151, 362-367.

- [3] Guo, Y., Li, S., Tawatsupa, B., Punnasiri, K., Jaakkola, J.J.K. and Williams, G. 2014. The association between air pollution and mortality in Thailand, *Scientific Reports*, 4, 5509 doi: 10.1038/srep05509.
- [4] Pinichka, C., Makka, N., Sukkumnoed, D., Chariyalertsak, S., Inchai, P. and Bundhamcharoen, K. 2017. Burden of disease attributed to ambient air pollution in Thailand: a GIS-based approach, *PLoS One*, 12, e0189909, doi: 10.1371/journal.pone.0189909.
- [5] Janjai, S., Suntaropas, S. and Nunez, M. 2009. Investigation of aerosol optical properties in Bangkok and suburbs, *Theoretical and Applied Climatology*, 96, 221-233.
- [6] Janjai, S., Nunez, M., Masiri, I., Wattan, R., Buntoung, S., Jantarach, T. and Promsen, W. 2012. Aerosol optical properties at four sites in Thailand, *Atmospheric and Climate Sciences*, 2, 441-453.
- [7] Levy, R.C., Mattoo, S., Munchak, L.A., Remer, L.A., Sayer, A.M., Patadia, F. and Hsu, N.C. 2013. The collection 6 MODIS aerosol products over land and ocean, *Atmospheric Measurement Techniques*, 6, 2989-3034.
- [8] Deng, X., Shi, C., Wu, B., Chen, Z., Nie, S., He, D. and Zhang, H. 2012. Analysis of aerosol characteristics and their relationships with meteorological parameters over Anhui province in China, *Atmospheric Research*, 109-110, 52-63.
- [9] Kumar, T.K., Gadhavi, H., Jayaraman, A., Suman, M.N.S. and Rao, S.V.B. 2013. Temporal and spatial variability of aerosol optical depth over south India as inferred from MODIS, *Journal of Atmospheric and Solar-Terrestrial Physics*, 94, 71-80.
- [10] Zhang, L., Zhang, M. and Yao, Y. 2019. Multi-time scale analysis of regional aerosol optical depth changes in national-level urban agglomerations in China using MODIS collection 6.1 datasets from 2001 to 2017, *Remote Sensing*, 11, 201, Available online: <https://doi.org/10.3390/rs11020201>.
- [11] Shen, Y., Zhang, L., Fang, X., Zhao, Z., Li, X., Wang, J. and Chai, Q. 2018. Long-term analysis of aerosol optical depth over the Huaihai Economic Region (HER): Possible causes and implications, *Atmosphere*, 9, 93, Available online: <https://doi.org/10.3390/atmos9030093>.
- [12] Floutsis, A.A., Korras-Carraca, M.B., Matsoukas, C., Hatzianastassiou, N. and Biskos, G. 2016. Climatology and trends of aerosol optical depth over the Mediterranean basin during the last 12 years (2002–2014) based on collection 006 MODIS-Aqua data, *Science of the Total Environment*, 551-552, 292-303.
- [13] Chen, Q.X., Huang, C.L., Yuan, Y., Mao, Q. J. and Tan, H.P. 2020. Spatiotemporal distribution of major aerosol types over China based on MODIS products between 2008 and 2017, *Atmosphere*, 11, 703, Available online: <https://doi.org/10.3390/atmos11070703>.
- [14] Mao, Q., Huang, C., Chen, Q., Zhang, H. and Yuan, Y. 2019. Satellite-based identification of aerosol particle species using a 2D-space aerosol classification model, *Atmospheric Environment*, 219, 117057.
- [15] Stirnberg, R., Cermak, J. and Andersen, H. 2018. An analysis of factors influencing the relationship between satellite-derived AOD and ground-level PM₁₀, *Remote Sensing*, 10, 1353, Available online: <https://doi.org/10.3390/rs10091353>.
- [16] Zheng, C., Zhao, C., Zhu, Y., Wang, Y., Shi, X., Wu, X., Chen, T., Wu, F. and Qiu, Y. 2017. Analysis of influential factors for the relationship between PM_{2.5} and AOD in Beijing, *Atmospheric Chemistry and Physics*, 17, 13473-13489.
- [17] Kloog, I., Koutrakis, P., Coull, B.A., Lee, H.J. and Schwartz, J. 2011. Assessing temporally and spatially resolved PM_{2.5} exposures for epidemiological studies using satellite aerosol optical depth measurements, *Atmospheric Environment*, 45, 6267-6275.
- [18] Lee, H.J., Coull, B.A., Bell, M.L. and Koutrakis, P. 2012. Use of satellite-based aerosol optical depth and spatial clustering to predict ambient PM_{2.5} concentrations, *Environmental Research*, 118, 8-15.
- [19] Cai, K., Li, S., Zheng, F., Yu, C., Zhang, X., Liu, Y. and Li, Y. 2018. Spatio-temporal variations in NO₂ and PM_{2.5} over the central plains economic region of China during 2005–2015 based on satellite observations, *Aerosol and Air Quality Research*, 18, 1221-1235.
- [20] Mao, X., Shen, T. and Feng, X. 2017. Prediction of hourly ground-level PM_{2.5} concentrations 3 days in advance using neural networks with satellite data in Eastern China, *Atmospheric Pollution Research*, 8, 1005-1015.
- [21] PCD. 2019. *Thailand State of Pollution Report 2018*, Pollution Control Department, Thailand. Available online http://pcd.go.th/file/Thailand%20Pollution%20Report%202018_Thai.pdf [Accessed on: 20 December 2020].
- [22] Bridhikitti, A. 2013. Atmospheric aerosol layers over Bangkok Metropolitan Region from CALIPSO observations, *Atmospheric Research*, 127, 1-7.
- [23] Kanabkaew, T. 2013. Prediction of hourly particulate matter concentrations in Chiangmai, Thailand using MODIS aerosol optical depth and ground-based meteorological data, *Environment Asia*, 6, 65-70.
- [24] Zeeshan, M. and Oanh, N.T.K. 2014. Assessment of the relationship between satellite AOD and ground PM₁₀ measurement data considering synoptic meteorological patterns and Lidar data, *Science of the Total Environment*, 473-474, 609-618.
- [25] Sukitpaneevit, M. and Oanh, N.T.K. 2014. Satellite monitoring for carbon monoxide and particulate matter during forest fire episodes in Northern Thailand, *Environmental Monitoring and Assessment*, 186, 2495-2504.
- [26] NSO. 2020. *Gross Provincial Product for Thailand, Greater Bangkok*. National Statistical Office, Thailand. Available online: <http://service.nso.go.th/nso/web/statseries/statseries15.html> [Accessed on: 23 September 2020].
- [27] EPPO. 2020. *Total Energy Consumption*. Energy Policy and Planning Office, Thailand. Available online <https://data.energy.go.th/output/consumption/search> [Accessed on: 23 September 2020].
- [28] NSO. 2020. *Registered Population for Thailand, Greater Bangkok, and Bangkok*. National Statistical Office, Thailand. Available online: <http://statbbi.nso.go.th/staticreport/page/sector/en/01.aspx> [Accessed on: 23 September 2020].
- [29] TMD. 2020. *Climate of Thailand*. Thai Meteorological Department, Thailand. Available online: https://www.tmd.go.th/en/archive/thailand_climate.pdf [Accessed on: 20 December 2020].
- [30] Aman, N., Manomaiphiboon, K., Pala-En, N., Kokkaew, E., Boonyoo, T., Pattaramunikul, S., Devkota, B. and Chotamonsak, C. 2020. Evolution of urban haze in Greater Bangkok and association with local meteorological and synoptic characteristics during two recent haze episodes, *International Journal of Environmental Research and Public Health*, 17, 9499, Available online: <https://doi.org/10.3390/ijerph17249499>.
- [31] Aman, N. 2019. *An Integrated Analysis of Visibility and Associated Factors over Selected Areas in Thailand*, Doctoral thesis, the Joint Graduate School of Energy and Environment, King Mongkut's University of Technology Thonburi.

- [32] PCD. 2003. *Particulate Matter Measurement*, Pollution Control Department, Thailand. Available online: <http://infofile.pcd.go.th/air/DustinAmbient.pdf> [Accessed on: 20 December 2020].
- [33] Saha, S., Moorthi, S., Pan, H.L., Wu, X., Wang, J., Nadiga, S., Tripp, P., Kistler, R., Woollen, J., Behringer, D., Liu, H., Stokes, D., Grumbine, R., Gayno, G., Wang, J., Hou, Y.T., Chuang, H.Y., Juang, H.M.H., Sela, J., Iredell, M., Treadon, R., Kleist, D., Delst, P.V., Keyser, D., Derber, J., Ek, M., Meng, J., Wei, H., Yang, R., Lord, S., Dool, H.V.D., Kumar, A., Wang, W., Long, C., Chelliah, M., Xue, Y., Huang, B., Schemm, J.K., Ebisuzaki, W., Lin, R., Xie, P., Chen, M., Zhou, S., Higgins, W., Zou, C.Z., Liu, Q., Chen, Y., Han, Y., Cucurull, L., Reynolds, R.W., Rutledge, G. and Goldberg, M. 2010. The NCEP climate forecast system reanalysis, *Bulletin of the American Meteorological Society*, 91, 1015-1058.
- [34] Saha, S., Moorthi, S., Wu, X., Wang, J., Nadiga, S., Tripp, P., Behringer, D., Hou, Y.T., Chuang, H.Y., Iredell, M., Ek, M., Meng, J., Yang, R., Mendez, M.P., Dool, V.D., Zhang, Q., Wang, W., Chen, M. and Becker, E. 2014. The NCEP climate forecast system version 2, *Journal of Climate*, 27, 2185-2208.
- [35] Giglio, L., Schroeder, W. and Justice, C.O. 2016. The collection 6 MODIS active fire detection algorithm and fire products, *Remote Sensing of Environment*, 178, 31-41.
- [36] Nichol, J.E. and Bilal, M. 2016. Validation of MODIS 3 km resolution aerosol optical depth retrievals over Asia, *Remote Sensing*, 8, 328, <https://doi.org/10.3390/rs8040328>.
- [37] Bilal, M., Nazeer, M., Nichol, J., Qiu, Z., Wang, L., Bleiweiss, M.P., Shen, X., Campbell, J.R. and Lolli, S. 2019. Evaluation of Terra-MODIS C6 and C6.1 aerosol products against Beijing, XiangHe, and Xinglong AERONET sites in China during 2004–2014, *Remote Sensing*, 11, 486, Available online: <https://doi.org/10.3390/rs11050486>.
- [38] Gupta, P., Remer, L.A., Levy, R.C. and Mattoo, S. 2018. Validation of MODIS 3 km land aerosol optical depth from NASA's EOS Terra and Aqua missions, *Atmospheric Measurement Techniques*, 11, 3145-3159.
- [39] Phairuang, W., Suwattiga, P., Chetianukornkul, T., Hongtieab, S., Limpaseni, W., Ikemori, F., Hata, M. and Furuuchi M. 2019. The influence of the open burning of agricultural biomass and forest fires in Thailand on the carbonaceous components in size-fractionated particles, *Environmental Pollution*, 247, 238-247.
- [40] Junpen, A., Pansuk, J., Kamnoet, O., Cheewaphongphan, P. and Garivait, S. 2018. Emission of air pollutants from rice residue open burning in Thailand, 2018, *Atmosphere*, 9, 449, Available online: <https://doi.org/10.3390/atmos9110449>.
- [41] Abdullah, S., Napi, N.N.L.M., Ahmed, A.N., Mansor, W.N.W, Mansor, A.A., Ismail, M., Abdullah, A.M. and Ramly, Z.T.A. 2020. Development of multiple linear regression for particulate matter (PM₁₀) forecasting during episodic transboundary haze event in Malaysia, *Atmosphere*, 11, 289, Available online: <https://doi.org/10.3390/atmos11030289>.
- [42] Vlachogianni, A., Kassomenos, P., Karppinen, A., Karakitsios, S. and Kukkonen, J. 2011. Evaluation of a multiple regression model for the forecasting of the concentrations of NO_x and PM₁₀ in Athens and Helsinki, *Science of the Total Environment*, 409, 1559-1571.
- [43] Tan, F., Lim, H.S., Abdullah, K. and Holben, B. 2016. Estimation of aerosol optical depth at different wavelengths by multiple regression method, *Environmental Science and Pollution Research*, 23, 2735-2748.
- [44] Jiang, C., Xu, Q., Gu, Y.K., Qian, X.Y. and He, J.N. 2018. Spatial and temporal changes of aerosol optical depth and its driving factors based on MODIS in Jiangsu province, *International Archives of the Photogrammetry, Remote Sensing and Spatial Information Sciences*, XLII-3, 645-649.
- [45] Aman, N., Manomaiphiboon, K., Pengchai, P., Suwanathada, P., Srichawana, J. and Assareh, N. 2019. Long-term observed visibility in eastern Thailand: temporal variation, association with air pollutants and meteorological factors and trends, *Atmosphere*, 10, 122, Available online: <https://doi.org/10.3390/atmos10030122>.
- [46] R Development Core Team. 2020. *R: A language and environment for statistical computing*. R Foundation for Statistical Computing. Available online: <https://www.r-project.org>. [Accessed on: 29 July 2021].
- [47] Shokoohinia, P., Assareh, N., Manomaiphiboon, K., Chusai, C., Kerkkaiwan, S., Unapumnuak, K. and Aman, N. 2020. Impacts of transboundary smoke haze from biomass burning in Lower Southeast Asia on air quality in southern Thailand, *Journal of Sustainable Energy and Environment*, 10, 1-10.
- [48] Paton, C.P. and Manomaiphiboon, K. 2013. A metropolitan wind resource assessment for Bangkok, Thailand part 1: Wind resource mapping, *Journal of Sustainable Energy and Environment*, 4, 69-76.